Renewable and Sustainable Energy Reviews 180 (2023) 113299

Contents lists available at ScienceDirect

Renewable and Sustainable Energy Reviews

journal homepage: www.elsevier.com/locate/rser

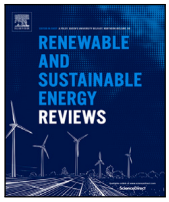

Original research article

Peak shaving control in OWC wave energy converters: From concept to implementation in the Mutriku wave power plant

A.A.D. Carrelhas *, L.M.C. Gato *, J.C.C. Henriques

IDMEC, Instituto Superior Técnico, Universidade de Lisboa, Av. Rovisco Pais 1, 1049-001 Lisboa, Portugal

ARTICLE INFO

Keywords:
Wave energy
Oscillating water column
Air turbine
PTO control
Peak shaving
Sea testing

ABSTRACT

Control algorithms for wave energy conversion technologies with air turbines require contingency tools to prevent the rated power and maximum rotational speed from being exceeded. Survival problems limit energy conversion when the available power is too large compared to the turbo-generator-rated power. Short-term predictions require information from local wave-measuring buoys, which raises reliability concerns. Wave groups in the ocean result in extremely high wave power peaks that cannot be smoothed by low-inertia power-take-off (PTO) systems, leading to survival problems. The most common strategy to cope with this situation is to set the rated power of the PTO several times more than the annual average produced electrical power. The PTO is shut-down when the available power is excessive. These two engineering decisions have a detrimental impact on the capacity factor and the energy cost. The paper shows a new control algorithm for wave energy oscillating-water-column (OWC) devices that can control the shutter position of a fast-acting valve to dissipate the pneumatic energy excess. Hence, the PTO can operate even when the available power is significantly larger than the generator's rated power. The algorithm was validated with the 30 kW biradial turbine prototype from the OPERA H2020 European project under real sea conditions at Mutriku's wave power plant. Results show the algorithm's effectiveness in real situations and during a generator failure simulated during the experimental campaign. This new concept may reduce the energy cost from wave energy and open a new field of design possibilities for OWC wave energy converters.

1. Introduction

In the last 30 years, climate change and its dreadful consequences have been debated and studied massively, leading to significant government efforts to take several mitigation actions over the years to stop it [1]. Not all countries are on the same step on the ladder, and developing countries have been making a hard path throughout economic growth with the same tools already developed countries used (and are using) [2]. Consequently, many international protocols have been signed over the last decades to overcome this issue that does not directly impact the final goal, which is to be possible for humankind to live on Planet Earth [3].

For most countries, the consequences of climate change are not yet in their backyard, which implies that national politics cannot deploy a lot of the annual expenditures on that sector to the detriment of others, such as health or education [4]. Nevertheless, recent events caused this subject to become a priority due to the possibility of a lack of energy supply. Countries minimise energy consumption and make significant investments and strategic planning for sustainable energy generation. Security of supply and energy independence is now a must-have [5].

The plan is to have a highly electrified, efficient, and low-carbon energy system [6]. Digitisation of all components connected in a smart grid will allow real-time control of the grid demand and supply of energy [7]. The upcoming regulation must adapt to the changing market conditions and disruptions to promote resilience in the sector [8]. Introducing new players in the liberalised market will decrease the final energy cost. Marine renewable technologies have potential competitive advantages over other mature renewable technologies in decarbonising activities that concern the ocean – the Blue Economy – such as shipping, ports [9], offshore aquaculture [10], oceanographic observations [11], remote islands [12] and power-to-gas [13]. Furthermore, it will help the path to decentralisation and boost existing local energy communities. This aligns with several of the Sustainable Development Goals set forth by the United Nations, namely, affordable and clean energy; decent work and economic growth; industry, innovation and infrastructure; sustainable cities and communities; and climate action.

* Corresponding authors.
E-mail addresses: ana.carrelhas@tecnico.ulisboa.pt (A.A.D. Carrelhas), luis.gato@tecnico.ulisboa.pt (L.M.C. Gato).

https://doi.org/10.1016/j.rser.2023.113299
Received 7 August 2022; Received in revised form 8 March 2023; Accepted 11 April 2023
Available online 2 May 2023

Nomenclature

Roman symbols

a	control law parameter [Nm s^b]
b	control law parameter [-]
D	rotor diameter [m]
e	normalised error of the P controller [-]
K_p	proportional gain of the P controller [-]
p	pressure [Pa]
P	power [W]
P_{gen}^{PSC}	generator power limit for controller [W]
Q	flow rate [m^3/s]
t	time[s]
T	torque [Nm]
u	HSSV normalised shutter position [-]

Greek symbols

Δ	variation, interval
Δp	turbine available pressure head [Pa]
η	efficiency [-]
Π	power, torque coefficient [-]
ρ	air density [kg/m^3]
Φ	flow coefficient [-]
Ψ	pressure coefficient [-]
Ω	rotational speed [rad/s]
Ω_{gen}^{PSC}	generator rotational speed limit for controller [rad/s]

Superscripts

–	average quantity
A–C	atmosphere to chamber
C–A	chamber to atmosphere
lim	limit
PSC	peak shaving control
rated	rated quantity

Subscripts

avail	available
bep	best efficiency point
ctrl	reference to valve position function
gen	generator
L	lower-threshold
max	maximum
rated	rated quantity
turb	turbine
U	upper-threshold

Acronyms

AMCA	Air Movement and Control Association
CAPEX	Capital Expenditures
DI	Digital Input
DO	Digital Output
H2020	Horizon 2020
HSSV	High-Speed Safety Valve
IST	Instituto Superior Técnico
OPERA	Open Sea Operating Experience to Reduce Wave Energy Cost
OPEX	Operational Expenditure
OWC	Oscillating Water Column
PSC	Peak Shaving Control
PEHD	Polyethylene High-density
P	Proportional
PLC	Programmable Logic Controller
PTO	Power Take-off System
WEC	Wave Energy Converter

Albeit extensive research and development programmes have been undertaken to foster a wave energy industry, the technology is still far from the maturity of more conventional renewable technologies [14]. The EU recognised this fact and provided several policy mechanisms to raise the competitiveness of the wave energy sector to the level of the wind and photovoltaic sectors [15]. Despite these efforts, wave energy has yet to reach the commercial stage. Two reasons for this failure are the harsh environment and the large peak-to-average power ratio associated with the randomness of the resource. They make the wave energy converter (WEC) design a unique engineering challenge compared with other renewable energies [16].

A standard parameter used to compare energy systems is the capacity factor. The capacity factor is the ratio between the electrical energy produced during one year and what would be produced annually if the system always performed at its rated power. The capacity factors of intermittent renewable energy technologies are relatively low compared to dispatchable generation such as biomass and geothermal power plants or coal, natural gas and nuclear power plants.

Direct comparison of wind turbines and WECs' capacity factors usually favour the wind turbine, and this is due to essential differences between the wind and the wave resources. Moreover, wind turbines can decrease their efficiency by blade-pitch and rotation speed control, limiting the electrical power output for wind speeds above a given rated wind speed, typically between 10 to 13 m/s. The cut-off wind speed is typically set above 25 m/s for the most recent large offshore wind turbines. Whereas wind power is proportional to the third power of the wind speed, this procedure allows the turbine to operate at the rated power between the rated wind speed and the cut-off wind speed, which provides capacity factors above 0.4. The variation of the average seasonal wave resource and the high wave power peaks produced by wave groups generally lead to wave energy converters capacity factors of about 0.25 or below.

Aiming to increase the capacity factor, the WEC operation under more energetic sea states is a critical issue that must be addressed at the design stage [17]. WECs are designed to withstand extreme storm conditions with a typical peak-to-average power ratio up to 30 [18]. This value provides the conditions for the mechanical design of the structural parts. Under normal operating conditions, the peak-to-average power ratio in the power take-off (PTO) system is much lower, typically from 7 to 10 [19]. This range of values is used for the mechanical design and control of the PTO system, as the power plant is shut down in wave storms for safety reasons.

There are various physical mechanisms whence energy can be extracted off waves, resulting in different WEC concepts. Based on the operating principle and morphological characteristics, these can be divided into four main groups: over-topping [20], membrane-pump [21], oscillating-body and oscillating-water-column (OWC) [22] devices. The first two are non-resonating WECs with water or air accumulated into a reservoir, giving moderate peak-to-average power ratio values in the PTO under normal operation [23] compared to the resonate oscillating-body and OWC WECs [24].

In the case of oscillating-body WECs, the PTO system or an additional dissipative system must withstand dynamic forces resulting from the more energetic sea states [25]. Stiff systems such as hydraulic

circuits or linear generators have structural problems when dealing with the peak stresses associated with large wave forces, especially for compressing stresses due to buckling. Furthermore, the cyclic nature of the wave forces causes significant fatigue and wear problems. These issues are not found in OWC WECs.

OWC are devices consisting of a fixed or floating hollow structure – the air chamber – open to the sea below the water surface confining air above the inner free surface [26]. The waves' action alternately compresses and expands the entrapped air in the chamber. The pressure difference between the air chamber and the atmosphere drives a self-rectifying air turbine [27].

Several types of self-rectifying turbines have been proposed, such as the Wells turbine [28], axial-impulse turbine [29], radial-impulse turbine [30], the biradial turbine [31] and twin-rotor turbine [32]. Ref. [33] provides a comprehensive review of the technology. Wells and axial-flow impulse turbines are the most popular self-rectifying turbines.

Compared to the expected mean for the site and device, the available energy to the PTO can be excessive in more energetic sea states. An over-rated capacity for the electrical generator could be selected to handle the large peak-to-average resource power ratio for the safe operation of the OWC PTO system. If the generator's rated capacity is sufficiently high, neither the rotational speed nor the generator power will be exceeded.

This design option has two disadvantages: (i) it increases the cost of the PTO as a higher-rated-capacity generator is comparatively expensive, and (ii) it reduces the efficiency of the conversion of mechanical energy into electrical energy since under the more frequent near average conditions, the power of the over-rated-capacity generator is very small, resulting in a low efficiency of this component.

Two types of valves can be applied to control the pneumatic power available to the air turbine of OWC devices [37]: (i) a bypass relief valve mounted in parallel with the turbine [37], see Fig. 1 a), or (ii) a valve installed in series with the turbine [38,39], see Fig. 1 b). The first solution is the most obvious concept, but the large area required to make it effective limits its application to the protection of the PTO, e.g., slow closing whenever the available resource energy is too large [34]. Fig. 1 a_3) shows the sliding-type relief valve installed on the roof of the air chamber of the Pico power plant. The second one was proposed by Stephen Salter, who designed and manufactured a high-speed safety valve (HSSV) for installation in series with a Wells turbine [35,36]. The operating mode of this valve is only fully closed or fully open. The Salter's HSSV had two possible types of operation (i) PTO system protection by closing the valve and, therefore, restricting the airflow into the turbine and (ii) latching control where the valve is fully closed or open to allow phase control [39]. The valve has a rubber membrane pneumatically operated by a piston moving inside the inner turbine duct with a time response of less than 0.1 s, see Fig. 1 b). The valve was designed for the Pico wave power plant [34], but its mechanical complexity and maintenance problems deterred its installation.

The biradial turbine overcomes the well-known Wells turbine limitations [40] for OWCs: highly efficient operation at high-pressure heads and smooth decrease in efficiency above the peak efficiency. The turbine is symmetrical, considering a mid-plane perpendicular to its axis of rotation. A pair of fixed guide-vane rows installed in a radial duct surrounds the rotor blades at the inlet and outlet. The biradial turbine geometry enables installing a built-in axially sliding mechanism that operates an HSSV whose typical stroke is around 10% of the turbine rotor diameter. The biradial turbine built-in HSSV is straightforward construction, reliable, much simpler and cheap than the membrane-based HSSV depicted in Fig. 1 b_1)–b_4). Although the HSSV introduces an additional moving part to the turbine, it allows a three-mode operation: (i) safety valve — an on/off mode aiming to protect the PTO and limit the turbine rotational speed, (ii) latching valve — for phase control, and (iii) high-speed partial closing.

The current paper explores and validates the possibility of performing a new type of control in an OWC WEC equipped with a biradial air turbine and an HSSV, allowing complete or partial closure. The authors' named peak shaving control (PSC) this new type of control for OWC with an HSSV valve able to partial closure. This control type is highly desirable as it alleviates the PTO mechanical loads and allows WEC operation in more energetic sea states, thus improving the capacity factor and grid integration. PSC also increases the mean efficiency of the electrical generator by allowing regular PTO operation with reduced rated power since the design limit to turbine available pneumatic power is never exceeded. It is a simple and effective mechanical energy dissipation method since it is a thermodynamic throttling process (a pressure loss in a valve).

PSC algorithm can be included in the category of OWC control with valves, so it requires simultaneous action on the electrical generator and the valve's shutter position. This work's primary goals are to understand (i) how the valve's partial shutter closure affects the turbine performance and (ii) how a control algorithm that uses the latter results can be devised for turbine-generator operation in real sea state conditions. Optimising the control variables of both PTO components is outside the scope of this paper.

Experimental testing of OWC PTO control algorithms has been made in hardware-in-the-loop (HIL) electrical test rigs [41] and in sea trials [42,43]. In an electrical HIL test rig, the WEC performance is numerically modelled in real-time as a function of the time-dependent prescribed incident wave field and the measured electrical generator rotational speed. At the same time, an electric motor applies the calculated instantaneous turbine shaft torque to the electrical generator [41]. The IST variable-flow test rig includes a real-time HIL flow controller, which allows experimental validation of the complete turbine-generator set performance in real-time under different control algorithms and realistic wave conditions [44,45].

The peak shaving control algorithm proposed in this paper was tested using the novel biradial air turbine for OWC applications built within the European H2020 OPERA project [46]. Two campaigns in different test rigs were performed: First, real conditions were mimicked at the IST variable flow test rig, allowing repeatability and reproducibility of flow conditions. Subsequently, tests were performed in real sea conditions at Mutriku's wave power plant.

This paper aims to answer the research question: May a peak shaving control algorithm be devised for OWC wave energy devices?

The contributions of the paper are: (1) the introduction of the new concept of peak shaving control for wave energy devices of the OWC type changing the current paradigm of these devices; (2) concept proof of the novel control algorithm with validation in dry testing at IST and under real sea conditions at Mutriku's wave power plant; (3) detailed analysis of the effect of the partial closure of the HSSV shutter on the performance of a biradial turbine; (4) demonstration that the novel control allows continuous operation even in the case of failure of the generator controller.

The structure of the paper is as follows. Section 2 describes the components of OPERA's PTO system. Next, the adopted strategy for the peak shaving control algorithm is presented in Section 3. The description of the two test rigs, including instrumentation and data acquisition systems, is introduced in Section 4. The discussion and analysis of results are followed by the conclusions and proposed future work in Sections 5 and 6, respectively.

2. Power take-off system

The PTO consists of (i) a biradial air turbine with fixed guide vanes, (ii) a high-speed safety valve (HSSV) and (iii) an electrical generator as schematically depicted in Fig. 2. Its main characteristics are presented in Table 1. A conical adapter was used to assemble the PTO at the IST variable flow test rig and Mutriku's wave power plant easily.

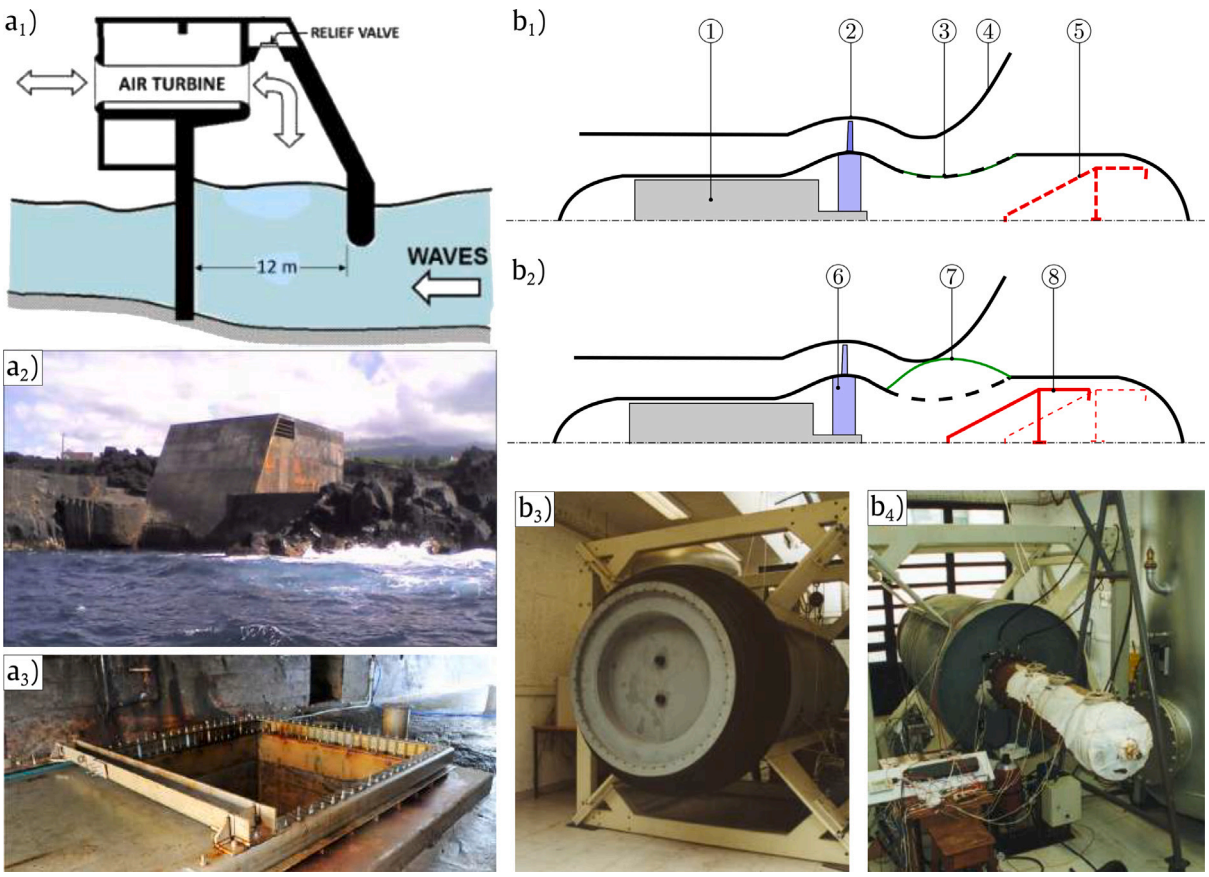

Fig. 1. Valve arrangement types. a) Relief valve mounted in parallel with the turbine: a_1) schematic view of the Pico power plant depicting the relief valve location, a_2) Pico plant view from the sea, a_3) low-speed slide gate relief valve installed on the air chamber roof of the Pico power plant (fully-open position) [34]. b) Salter's high-speed safety valve (HSSV) in series with a Wells turbine: b_1) membrane shutter contracted (open position) and b_2) membrane shutter inflated (closed position), adapted from [35]. Labels: (1) - generator, (2) - spherical casing, (3) - membrane shutter contracted, (4) - duct, (5) - piston position for contracted membrane, (6) - Wells turbine rotor, (7) - membrane shutter inflated, (8) - piston (position for inflated membrane), b_3) and b_4) front and rear views of the Salter's HSSV Pico plant prototype with the membrane partially inflated during testing at IST [36].

Table 1
PTO main characteristics.
Source: Reproduced from [31].

Turbine-generator set		High-speed safety valve	
Air turbine	biradial		
Assembly position	vertical axis	Safety valve type	high-speed
Rated power, P_{gen}^{rated} [kW]	30	Valve type	cylindrical
Maximum speed, Ω_{max} [rad/s]	314	Shutter material	low friction PEHD
Turbine rotor diameter D [m]	0.50	Valve operating system	linear actuators
Maximum generator counter torque, T_{gen}^{lim} [Nm]	256	Number of actuators	4
Nozzle/Diffuser channel width [m]	0.053	Actuator unit rated capacity [kN]	1
Turbine stator diameter [m]	2.10	Protection index of actuators	IP65
Stator design	4×64 fixed guide vanes	Fast acting speed [m/s]	0.3
Turbine rotor inertia [kg m^2]	5.01		

The turbine is a biradial turbine with fixed guide vanes with a new stator design [47]. The adopted design prevents high stagnation pressure losses at the outlet guide vane system that generally penalises self-rectifying impulse turbines [27]. This is achieved by introducing a radial offset of the guide vanes from the rotor and replacing the usually single vane row, on each side of the rotor, with two concentric rows of guide vanes. The double row of guide vanes gives wider circumferential spacing for the exit flow while appropriately deflecting the flow admitted to the rotor [48].

The generator is a squirrel-cage induction electrical machine controlled by a variable-frequency drive with four quadrants, allowing torque or speed control. This paper refers to work performed at the IST Laboratory and Mutriku's wave power plant during the PTO's commissioning tests performed by the IST Team, from May to June 2017, within the framework of the H2020 OPERA project [46]. In these two OPERA project phases, the turbine-generator set was grid connected at the IST Laboratory and Mutriku's wave power plant through a 37 kW four-quadrant variable-frequency drive Siemens SINAMICS G120 regenerative power module PM250. Another variable frequency drive was used during the experimental campaigns that followed this work: see (i) the project reports concerning the testing at the Mutriku Wave Power Plant [49] and at the MARMOK-A-5 device [50]; and (ii) the comparative assessment of the turbine performance of the Wells and the biradial turbine at the Mutriku Wave Power Plant [19].

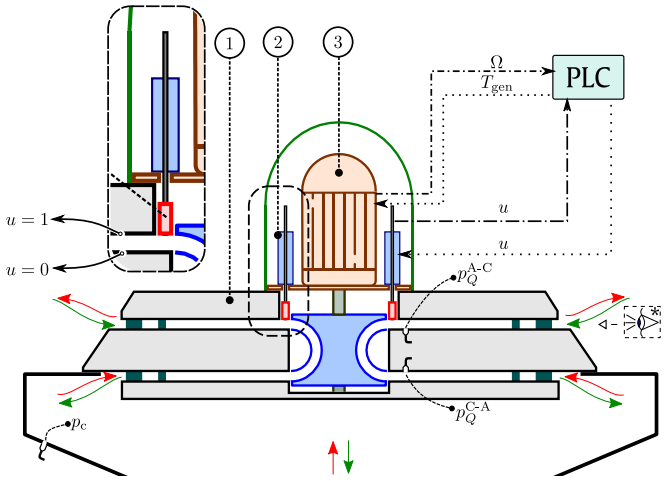

Fig. 2. Schematic representation of the PTO, detailed view of the high-speed safety valve (HSSV) (if the valve is open (closed) then $u = 1$ ($u = 0$)) and the input/output signals for the control algorithm using a PLC. The green and red arrows represent the flow direction. Labels 1, 2 and 3 indicate the biradial air turbine with fixed guide vanes, the high-speed safety valve and the electrical generator, respectively. Labels p_c, $p_Q^{A\text{-}C}$ and $p_Q^{C\text{-}A}$ denote the pressure taps' position to measure the air chamber pressure and the pressure for the flow rate calculation. The label marked with $*$ represents the perspective of the photographs shown in Fig. 4.

The HSSV is composed by two main component types: (i) a low friction PEHD annular ring with inner and outer diameters of 510 mm and 600 mm, respectively, and (ii) four linear actuators radially disposed at 90°. The linear actuators have a displacement encoder allowing closed-loop feedback control so that the position of the valve is accurately set and always known. Fig. 3 shows a photograph of the HSSV in its supporting structure during preliminary tests before installation into the PTO system.

Due to assembly and maintenance reasons, the valve is located in the stator closest to the generator atmosphere side); see Fig. 2. The total displacement of the HSSV shutter is 53 mm (the span between the two metal walls that compose the stator). Given the shutter speed of 0.3 m/s, the valve closes in less than 0.18 s. We define u as the variable that expresses the position of the HSSV shutter. It is $u = 1$ ($u = 0$) if the valve is open (closed), see the top-left corner of Fig. 2. A perspective of the stator in the atmosphere side during operation is shown in Fig. 4 (see label $*$ in Fig. 2). Four shutter positions are shown. In Fig. 4 a) the HSSV is fully open. In the following figures, the HSSV is gradually being closed. The white PEHD annular ring is the HSSV shutter. In Fig. 4 d) the HSSV is fully closed.

3. Control strategy

The control strategy is divided into two levels: electrical generator control and HSSV control. Both levels work independently of each other. They are shown in Fig. 5 a) and b) respectively, and are analysed below.

In what concerns the electrical generator control, the starting point of the control law design is based on the evidence that maximum energy production of an OWC WEC device is reached for an ideal turbine-generator set with zero inertia and constant electrical generator efficiency, if the instantaneous rotational speed, $\Omega(t)$, is controlled such that the instantaneous generator counter torque is [37]

$$T_{gen}(t) = \Pi_{bep}\rho\Omega^2(t)D^5\,. \tag{1}$$

Here ρ is the air density, Π_{bep} is the power coefficient corresponding to the turbine's maximum efficiency under steady-state conditions, and D is the turbine rotor's diameter. Under the above ideal assumptions, the PTO would respond instantaneously to the torque control set-point

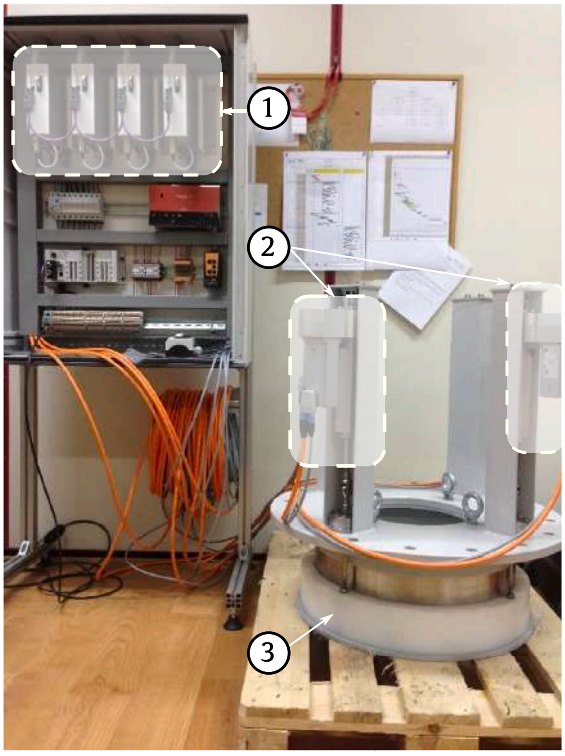

Fig. 3. High-speed safety valve (HSSV) in its supporting structure: 1 - actuators' controllers CMMP-AS-C2-3A-M0; 2 - linear actuators FESTO EPCO; 3 - annular shutter. See Fig. 2 to localise the HSSV in the PTO.
Source: Courtesy of Kymaner [51].

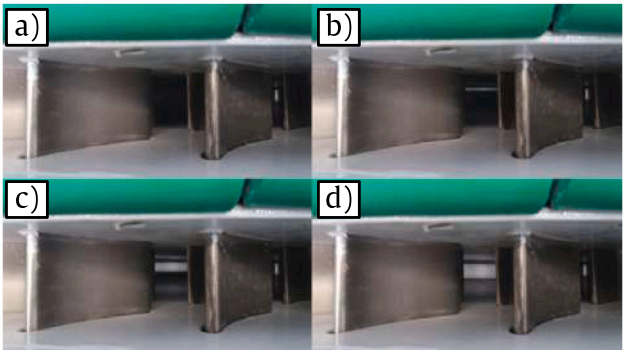

Fig. 4. Photographs of the biradial turbine stator in the atmosphere side during the high-speed safety valve (HSSV) operation. The white annular ring is the HSSV shutter. a) HSSV fully open; b)/c) partially closed; d) fully closed.

to an upcoming difference in pressure inside the pneumatic chamber. Although this situation is highly benign from the quantity of energy conversion point of view, it would harm the quality of the produced electrical energy due to the high instantaneous power variation. However, an actual device has inertia (due to the turbine, generator and other rotating masses, e.g., couplings), and the generator's efficiency depends on the applied load. So, a more general control law is used,

$$T_{gen}(t) = a\Omega^b(t)\,, \tag{2}$$

where the control parameters a and b are selected to maximise the PTO's energy conversion for given inertia and PTO damping introduced into the WEC hydrodynamics [52]. Given the generator's electrical power limit P_{gen}^{PSC} and maximum torque T_{gen}^{lim}, the generator counter

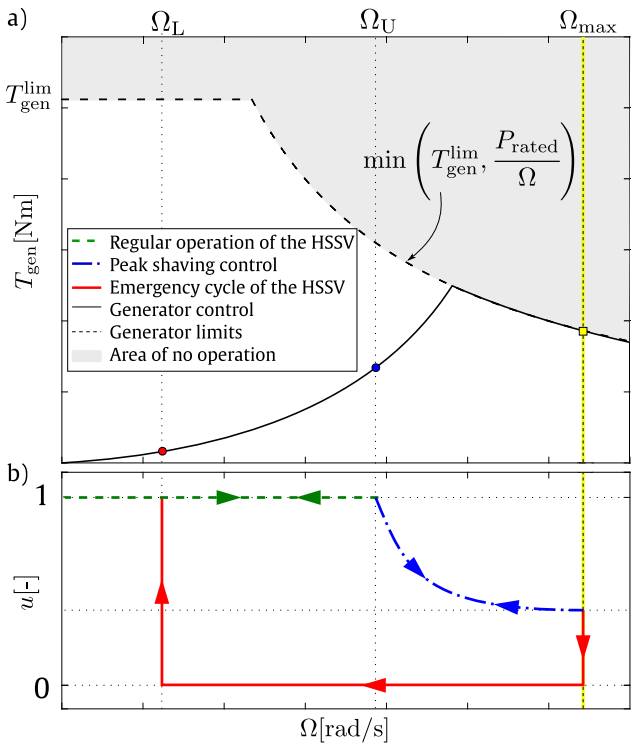

Fig. 5. Peak shaving control (PSC): electrical generator counter torque, T_{gen}, and high-speed safety valve (HSSV) shutter position, u, as a function of the turbine rotational speed, Ω – a) generator control and b) HSSV shutter position control.

torque is

$$T_{gen}(t) = \min\left(a\Omega^b(t), P_{gen}^{PSC}/\Omega(t), T_{gen}^{lim}\right). \quad (3)$$

The amount of available energy supplied to the PTO in regular operation allows safe operation. The HSSV is fully open, $u = 1$, if the instantaneous rotational speed is below an upper threshold, $\Omega(t) \leq \Omega_U$, see Fig. 5. When the available power is higher, the rotational speed increases due to the generator control law applied; see Eq. (3). If $\Omega(t) > \Omega_U$, the algorithm enters in PSC, and the HSSV partially closes ($0 \leq u \leq 1$) to respect the electrical generator power PSC setting value P_{gen}^{PSC} and not exceeding maximum rotational speed Ω_{max}^{PSC}. The control algorithm switches to regular operation when the instantaneous rotational speed is lower or equal to a lower threshold, $\Omega(t) \leq \Omega_L$. The values of Ω_L and Ω_U are determined using an optimisation algorithm to maximise the annual electricity production as described in Ref. [52].

The HSSV shutter position was controlled using a proportional (P) controller defined as

$$v_{ctrl} = K_p\, e(t). \quad (4)$$

Here $e(t)$ is the normalised error defined as

$$e(t) = \frac{\Omega(t) - \Omega_U}{\Omega_{max}^{PSC} - \Omega_U}, \quad (5)$$

and K_p is the non-negative gain of the proportional term, Fig. 6. A proportional–integral–derivative controller was initially considered, and valve-shutter-position control laws were compared using the same pressure time series. Whenever the rotational speed fluctuations were too fast, the integral controller suffered windup problems, and the derivative controller over-predicted the system response. As such, the integral and derivative gains were set to zero, turning into a P controller.

The flow rate Q across the HSSV is a non-linear function of its closure fraction. To cope with this non-linear behaviour, the response

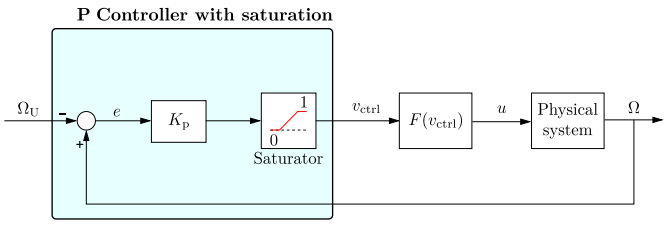

Fig. 6. High-speed safety valve (HSSV) shutter position controller.

of the P controller was changed by applying a monotonic decreasing function $F(v_{ctrl})$ such that

$$u(v_{ctrl}) = \begin{cases} 0 & v_{ctrl} \leq 0 \\ F(v_{ctrl}) & 0 < v_{ctrl} < 1 \\ 1 & v_{ctrl} \geq 1 \end{cases}. \quad (6)$$

Using the function $F(v_{ctrl})$ allowed testing different valve closure strategies without changing the P controller.

The dash-dotted blue line in Fig. 5 exemplifies the implementation of the PSC with the HSSV partial closure ($0 \leq u \leq 1$). If the maximum rotational speed, Ω_{max}, is attained, the HSSV closes, $u = 0$, and remains closed until $\Omega(t) \leq \Omega_L$.

As can be seen, there are several variables to be optimised. The objective is to minimise the actuation of the valve and maximise the produced energy while respecting the PTO's constraints (e.g., maximum rotational speed, Ω_{max}^{PSC}, electrical generator power PSC setting value, P_{gen}^{PSC}, and linear actuators wear).

4. Description of the test rigs

The experimental tests were performed in two test rigs: at the (i) IST variable flow test rig in Lisbon, Portugal and (ii) Mutriku's wave power plant in the Basque Country, Spain, see Fig. 7. The first test rig allows safe operation and repeatability conditions, and the second allows proper PSC validation in real sea state conditions. The following subsections describe detailed information about each test rig, instrumentation, and data acquisition system.

4.1. IST variable flow test rig

The PTO was tested at the variable flow test rig with the either steady-state or variable unidirectional flow, depending on the test. The test rig is an open circuit blow-down type test rig. The air temperature variation is assumed insignificant since the laboratory is adequately ventilated, and its volume is much larger than the one that passes throughout the test rig per minute. The test rig is schematically represented in Fig. 7 a$_1$). The PTO (1) is connected to an adapting antechamber (2) by the conical adapter. The adapting antechamber is connected to the first plenum chamber (3) whose purpose is to reduce the kinetic energy close to zero. At the exit of the first plenum chamber, there is a duct filled with a honeycomb lattice (4) that straightens the flow before entering the calibrated converging nozzle (6) for flow rate measurements. It is followed by a diffuser (7) to recover part of the kinetic energy and a second plenum (8) chamber designed to attenuate high-frequency pressure waves produced during the variable flow tests. Both plenum chambers, converging nozzle, and diffuser, were designed following the AMCA 210/99 Standard [54]. A 55 kW rated power radial fan (9) provides the pressure head across the turbine and is controlled by a variable frequency drive. A fast-acting valve (10) is assembled at the fan's exit, and a linear motor actuates it. The calibration methodology of the test-rig valve is described in [44] and was performed accordingly for the presented experimental tests.

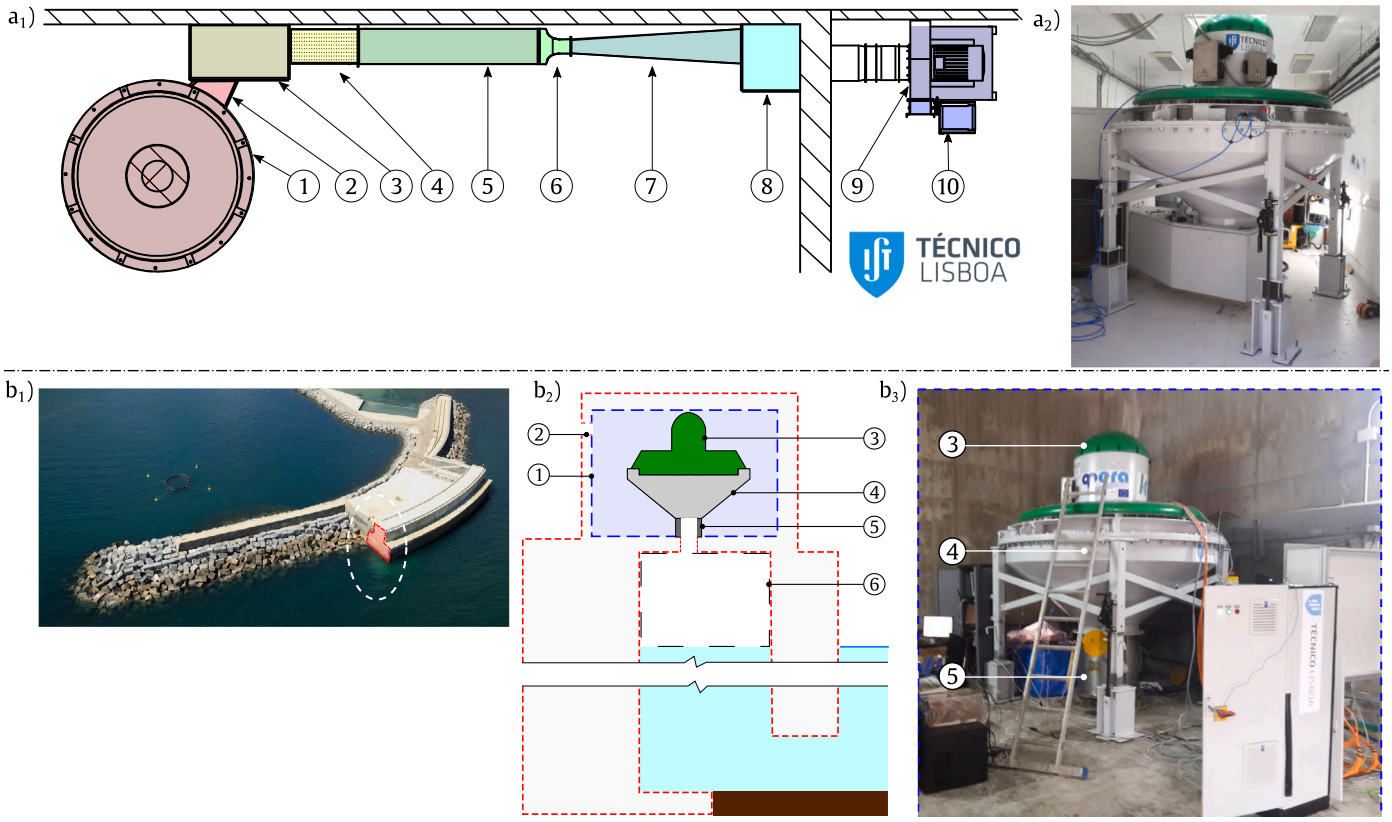

Fig. 7. Test rigs. a) IST variable flow test rig – a_1) top-view of the test rig: (1) PTO, (2) adapting antechamber, (3) first plenum chamber, (4) honeycomb lattice, (5) duct, (6) flow nozzle, (7) diffuser, (8) second plenum chamber, (9) 55 kW radial fan, (10) fast-actuating air valve (reproduced from [31]); a_2) PTO assembled into the laboratory. b) Mutriku's wave power plant: b_1) bird's eye view of the plant; b_2) side section schematic view of one pneumatic chamber (not to scale, the height is considerably larger when compared with the width [53]); b_3) photograph of the turbine's gallery: (1) turbine's gallery, (2) opening to the atmosphere, (3) PTO, (4) conical adapter, (5) interface duct, (6) pneumatic chamber.

4.2. Mutriku's wave power plant

The Mutriku wave power plant is built on a breakwater structure with approximately 440 m length [53]. It was constructed in 2011 to protect the Mutriku harbour in Basque Country, Spain. A gallery encloses the apertures to sixteen OWC chambers where circular ducts connect Wells turbines with a rated power of 18.5 kW, see Fig. 7. The OPERA's PTO was assembled into chamber nine throughout the conical adapter. The butterfly valve installed into the circular duct allows shut-down of the airflow if needed.

4.3. Instrumentation

The turbine pressure head, Δp, was measured with a KELLER PD-23 pressure sensor with pressure range 0 – 20 kPa and accuracy of ±0.5% of the full scale. This sensor measured the relative pressure between the atmosphere and a pressure tap at the conical adapter wall, labelled p_c in Fig. 2.

The turbine flow rate, Q, is calculated from the calibration performed at IST of the relation between the pressure of the tap closest to the rotor relative to the atmosphere, $p_Q^{A\text{-}C}$, and the flow rate measured by the test rig calibrated flow meter, see item (6) in Fig. 7 a_1). Similarly to the turbine pressure head measurements, KELLER PD-23 pressure sensors were used for the $p_Q^{A\text{-}C}$ measurements. A Honeywell HSCSNBN-001P-DAA5 pressure transducer with a range ±6.8 kPa, and 0.25% full-scale accuracy was used to measure the pressure drop at the test rig calibrated flow meter. This instrument was previously calibrated against a Betz micro-manometer, with absolute accuracy of 0.05 mmH_2O. It was found that the flow meter pressure drop is independent of the turbine rotational speed [31]. The turbine experiences different airflow directions depending on if the OWC free surface is increasing or decreasing its position relative to the sea bottom, see Fig. 2. If it increases (see red arrows), air compression inside the pneumatic chamber generates the flow throughout the turbine. First, it passes by the stator, follows the rotor, and then another stator before entering the atmosphere. If it decreases (see green arrows), air suction inside the pneumatic chamber drives the flow in the symmetric path to the previous situation. Thus, this implies that depending on the relative pressure inside the Mutriku's power plant pneumatic chamber, either the pressure-tap labelled $p_Q^{A\text{-}C}$ or $p_Q^{C\text{-}A}$ was used for the calculation of the flow rate, see Fig. 2.

The rotational speed, Ω, was measured by a Siemens encoder 1XP8012-1X HTL assembled into the generator shaft and calibrated at IST with a tachometer Graham & White model PT331, with absolute accuracy of 0.05 rpm.

The turbine torque, T_{turb}, was calculated from the previous calibration data of the electrical generator at IST, measuring the generator power with a power analyser and the rotational speed with the encoder mentioned above, as described in [31]. Note that a torque meter assembly in an industrial prototype is unreliable. A torque meter is a sensible instrument used in laboratory benches with tight tolerances and slight vibrations. Therefore, its use in applications such as floating WECs (the final destination of OPERA's prototype) would most likely deteriorate the sensor.

The air density, ρ, was calculated by measuring wet and dry temperatures and atmospheric pressure. Temperatures were measured with an accuracy of 0.5°C. A digital barometer with an accuracy of 0.1 mmHg

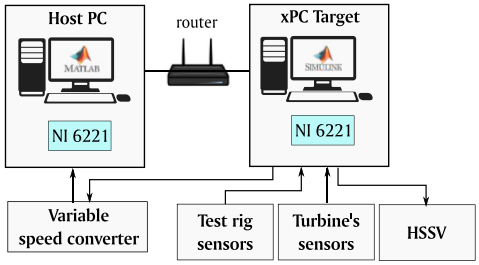

Fig. 8. Schematic representation of the data acquisition system used in the tests. *Source:* Reproduced from [31].

recorded the atmospheric pressure. The air density calculation follows the recommended procedure in AMCA 210-99 Standard [54]. In Mutriku's wave power plant, it was assumed that the air density is approximately the same inside the turbine's gallery and the pneumatic chamber.

The HSSV linear actuators are controlled with Festo CMMP-AS-C2-3A-M0 control modules commanded by a Programmable Logic Controller (PLC). The control modules receive signals from the PLC. There are eight DI/DO available slots on this PLC. Two define the control mode (mode 1 - fully open/closed; mode 2 - allow partial closing), and the remaining six determine the position of the valve with one-millimetre discretisation. Preliminary tests showed that the current supplied to the HSSV linear actuators exceeded the established design safety limit of 2.4 A (230 V AC) for a steady position below 40% of the valve's aperture. Therefore, the aperture was limited to $0.4 \leq u \leq 1$ to respect the maximum design actuating force of the OPERA's shutter actuators. When the valve is partially closed, the flow accelerates, decreasing the pressure on the inner cylindrical shutter surface and increasing the force acting upon the valve shutter. For this specific project, a decision was made regarding the components that constitute the HSSV based on the expected lifetime of the project. In future prototypes, further investigation on other types of actuators is recommended to endure the conditions met on the deployment site.

4.4. Data acquisition

A schematic representation of the data acquisition system is presented in Fig. 8. The system comprises two subsystems: (i) acquisition of the signals that enable the measurement of the generator electrical power output and (ii) acquisition of the remaining signals and control signals set-points (e.g., the position of the valve shutter and generator counter torque). The latter includes the test rig and PTO instrumentation. The first subsystem was configured on a Host PC with a Session-Based Interface. The second one was set throughout a Simulink Real-Time on an xPC Target. The use of signal triggers synchronised both subsystems, and PCI NI-6221 data acquisition boards were used.

5. Results

This section contains two subsections: results from the dry testing at IST in Section 5.1 and sea trial results at Mutriku's wave power plant in Section 5.2. Evaluating how the HSSV shutter position affects the turbine's performance is required to perform PSC. This analysis is presented in Section 5.1.1. The design of the auxiliary parametric function, $F(v_{\text{ctrl}})$, in Eq. (6) is described in Section 5.1.2 together with its validation tests. The validation test of PSC at IST variable flow test rig is shown in Section 5.1.3. Section 5.2.1 presents the PSC tests at the Mutriku wave power plant. As an ultimate test of the robustness of the PSC algorithm, Section 5.2.2 contains test results in an emergency case where the generator controller fails (zero generator's counter torque). Section 5.3 addresses the possible road to industrialisation and future work to improve the studied approach.

Table 2
Measured values for $\Phi_{\eta=0}$, $\Phi_{\eta_{\max}}$ and $\eta_{\max}$ for discrete positions of the HSSV.

u[−]	$\Phi_{\eta=0}$[−]	$\Phi_{\eta_{\max}}$[−]	$\eta_{\max}$[−]
1	0.05	0.115	0.70
0.7			0.63
0.5			0.45
0.4			0.32

5.1. IST variable flow test rig results

5.1.1. Turbine performance

The turbine performance is determined under steady-state flow. The electrical generator and motor's fan operate in speed-control mode when a constant rotational speed is set. The goal is to assess the relationship between the turbine pressure head coefficient,

$$\Psi = \frac{\Delta p}{\rho \Omega^2 D^2}, \tag{7}$$

flow coefficient,

$$\Phi = \frac{Q}{\Omega D^3}, \tag{8}$$

power coefficient,

$$\Pi = \frac{T_{\text{turb}}}{\rho \Omega^2 D^5}, \tag{9}$$

and efficiency,

$$\eta = \frac{\Pi}{\Phi \Psi}, \tag{10}$$

for a given constant rotational speed (set by the electrical generator) and turbine pressure head (set by the fan). The tests were performed for a range of rotational speed and Reynolds number of $495 \text{ rpm} \leq \Omega \leq 2595 \text{ rpm}$ and $2.1 \times 10^5 \leq \text{Re} \leq 1.3 \times 10^6$, respectively, corresponding to a range of flow coefficient of $0.05 \leq \Phi \leq 0.56$. The minimum rotational speed was 495 rpm due to the low efficiency of the generator for rotational speeds below that value [31]. The flow coefficient was set for values in the above range, from zero to maximum and then to zero, for all the rotational speeds. The maximum value of the flow coefficient was limited by the available power given by the test rig. Each test recorded all the needed variables to access the turbine's aerodynamic characteristics for 30 s. Fig. 9 displays the performance curves as a function of the flow coefficient for four different positions of the HSSV shutter, $u = 1$, 0.7, 0.5 and 0.4 (note that $u = 1$ is fully open and $u = 0$ is fully closed).

Analysis of Fig. 9 shows low dispersion of the measurements for all the presented coefficients (η, Π, Ψ), validating the dynamic similarity analysis and indicating a consistent experimental procedure. Inspection of the efficiency curves reveals how curves change their shape as a function of the HSSV shutter position: in a marginal way for high apertures, strongly as the aperture is reduced. Above $u = 0.5$, the curve begins to change its original form slightly. Values of $\Phi_{\eta=0}$ and $\Phi_{\eta_{\max}}$ are approximately constants in the tested aperture range. As expected, the maximum efficiency decreases as the aperture decreases. Table 2 presents the values for the abovementioned variables.

As for the efficiency curves, the HSSV shutter position modifies the curve $\Psi(\Phi)$. A higher available pressure head is required to provide a constant turbine flow rate value as the HSSV closes, steepening the quadratic relationship between the flow rate and pressure inside the turbine.

Values from Table 2 indicate that $\eta_{\max}$ decreases as the HSSV closes. Initially, the efficiency is barely affected by the valve's shutter position, following a substantial decrease as u approaches zero. The behaviour of the variables mentioned above is intrinsically connected. Because the power coefficient curve, $\Pi(\Phi)$, is unaffected, $\Phi_{\eta=0}$ and $\Phi_{\eta_{\max}}$ remain almost constant independently of u. This non-intuitive result demonstrates that the valve produces local flow losses, and the

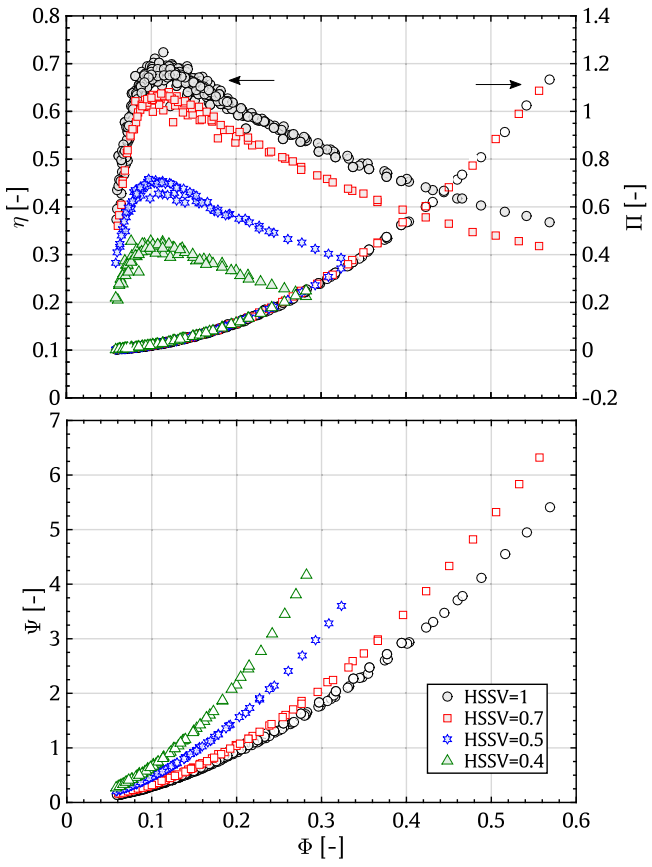

Fig. 9. Performance curves of the turbine: efficiency, power and pressure coefficient as a function of the flow coefficient for four different HSSV shutter positions, u = 1, 0.7, 0.5 and 0.4.

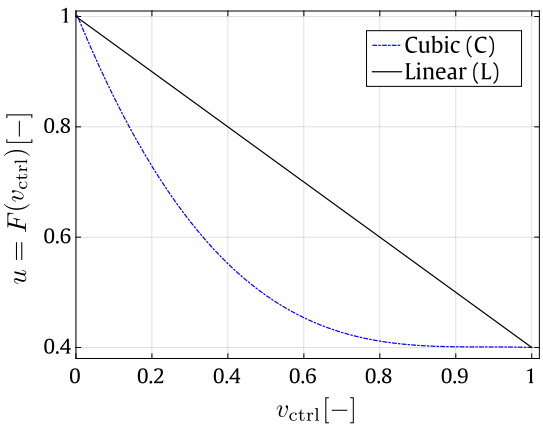

Fig. 10. The two tested parametric control functions $F(v_{ctrl})$.

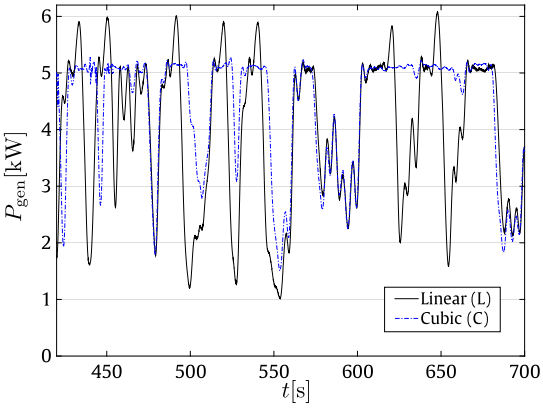

Fig. 11. Tests for a control law: $a = 1.11\times10^{-3}$ Nms^2, $b = 2$, $P_{gen}^{PSC} = 5$ kW, $T_{gen}^{lim} = 256$ Nm, $\Omega_U = 100$ rad/s and $\Omega_L = 50$ rad/s, with auxiliary parametric functions L and C.

angular momentum of the flow leaving the rotor remains approximately the same. Therefore, the energy per unit mass exchanged between the rotor and the fluid remains approximately constant. However, the rotor efficiency decreases due to incidence losses at the entry of the rotor owing to flow separation downstream of the valve's shutter. From the rotor's point of view, the valve produces a local head loss, not affecting the angular momentum of the flow at the rotor exit. Note that the same valve configuration in other turbine types may have a different effect. This feature of the biradial turbine rotor is due to its blade design forming long flow channels required to provide enough guidance to turn the inlet centripetal flow into the exit centrifugal flow [48,55]. Also, note that the PSC objective is to dissipate excess pneumatic energy from sea states with mean available power much larger than the generator's rated power using the HSSV partial aperture. Maximising the turbine's efficiency is not a goal in excessively energetic sea states.

5.1.2. HSSV control algorithm under peak shaving control

The PSC implies the design of a control sub-algorithm for the HSSV aperture. From the results in Fig. 9, the variation of the turbine peak efficiency as a function of the HSSV shutter position u is obtained (see Table 2). It can be seen that η_{max} decreases as an approximately cubical polynomial when the HSSV closes. The decrease in the maximum efficiency is higher (lower) when the valve approaches (is far from) the closed position. Based on this evidence, an aggressive (smooth) valve control law is needed for lower (higher) values of u.

Two valve shutter position control laws $F(v_{ctrl})$ were considered: a linear law (L) and a cubic law (C) that was designed to achieve an almost linear variation of the flow rate across the HSSV as a function of v_{ctrl}, see Fig. 10. These control laws were compared using the same imposed pressure time series. The proportional gain of the P controller was set so that $K_p = 1$.

For this subsection and forward, the generator operates in generator mode. As discussed in Section 3, the proposed PSC algorithm has several variables to consider. The current work focuses on validating the effectiveness of this valve type for PSC in PTOs for OWC applications. As such, for the current Subsection, the generator's control parameters in Eq. (3) are shown in Table 3, see Section 3. The goal is to understand the robustness of the PSC algorithm for the turbine not exceeding electrical generator power PSC setting value P_{gen}^{PSC} nor the maximum rotational speed, Ω_{max}^{PSC}. Fig. 11 depicts the generator's electrical power output time-series using the two functions $F(v_{ctrl})$ depicted in Fig. 10.

Results in Fig. 11 show that the valve's control parametric cubic function C was able to protect the generator from exceeding the electrical generator power PSC setting value of P_{gen}^{PSC} = 5 kW. This can be seen by analysing the variation of the generator power depicted in a dashed-dot blue line. On the contrary, the parametric control function L is not suitable because the obtained generator power peaks vastly exceeded the prescribed limit, e.g., between t = 500 s and t = 550 s.

5.1.3. Peak shaving control test implementation: variable unidirectional flow

Using the auxiliary parametric function C, another set of tests was performed imposing the same pressure time series but with lower electrical generator power PSC setting values: P_{gen}^{PSC} = 2 kW and P_{gen}^{PSC} = 3 kW. Eq. (3) gives the generator control law with the corresponding parameters presented in Table 3.

Table 3
Control algorithm parameters for validation tests at both IST variable flow test rig (IST) and Mutriku's wave power plant (Mutriku). Here, $T_{gen}^{lim} = 256\,Nm$. The values of the variables $a = 1.11 \times 10^{-3}\,Nm\,s^2$ ($a = 3.50 \times 10^{-4}\,Nm\,s^{2.32}$) and $b = 2$ ($b = 2.32$) correspond to the ideal turbine-generator set with zero inertia and constant electrical generator efficiency, see Eq. (1) (maximum turbine power for the sea state during this specific test accordingly to the numerical simulations presented in [56]).

Test rig	$a \times 10^4$ [Nm s^b]	b [–]	Ω_L [rad/s]	Ω_U [rad/s]	Ω_{max}^{PSC} [rad/s]	P_{gen}^{PSC} [kW]	$\overline{P}_{avail}$ [kW]	Subsection/ Figure
IST	11.1	2.00	100	130	195	5	6.5	5.1.2/11
IST	11.1	2.00	50	122	187	2	6.5	5.1.3/12 a)
				139	204	3		
Mutriku	11.1	2.00	180	230	295	30	14.6	5.2.1/12 b)
	3.5	2.32	150	176	241	10	7.9	
Mutriku	0	–	150	230	250	0	3.5	5.2.2/13
	0	–	190	230	250	0	4.4	

Fig. 12 a) depicts the generator's instantaneous power, rotational speed and HSSV shutter normalised position u time series. Inspection of Fig. 12 a) demonstrates that the generator power P_{gen}^{PSC} was successfully limited in all tests. The oscillations of each test relative to the imposed electrical generator power PSC setting value are negligible. These might be brought on by how accurately the sensors measured the generating power. The number of times the HSSV has actuated decreases, whereas the actuation time increases as the imposed rated power decreases. For control law with $P_{gen}^{PSC} = 3\,kW$, the valve varies its aperture between fully open and 40% closed ($0.4 \leq u \leq 1$). Note that the HSSV was never fully closed in any test, reinforcing the robustness of the presented control since it effectively decreased the turbine's available power. Hence, the PTO can operate in very energetic sea states. Although the control had been validated in the IST test rig, the same may still need to be confirmed at Mutriku's wave power plant. Since the flow is bidirectional, the performed tests did not include the situation where the HSSV is at a position that throttles the flow exiting the rotor. Therefore, there is likely a need to adjust the control algorithm at Mutriku's plant.

5.2. Mutriku wave power plant results

5.2.1. Peak shaving control test implementation: real conditions

Results for two tests with the control algorithm variables presented in Table 3 are plotted in Fig. 12 b). This figure displays the generator power, valve shutter normalised position, rotational speed, and available power time series.

Inspection of Fig. 12 b) reveals that neither the imposed electrical generator power PSC setting value, P_{gen}^{PSC}, nor the maximum rotational speed, Ω_{gen}^{PSC}, was exceeded in any tests. When the value of generator power is $P_{gen}^{PSC} = 10\,kW$, the valve position change with time more intensively than when $P_{gen}^{PSC} = 30\,kW$. There are two causes for this difference: the ratio between the average available pneumatic power ($\overline{P}_{avail}$) and the imposed electrical generator power PSC setting value, P_{gen}^{PSC}. As indicated in Table 3, $\overline{P}_{avail}/P_{gen}^{PSC} = 0.79$ in the test case with $P_{gen}^{PSC} = 10\,kW$, whereas $\overline{P}_{avail}/P_{gen}^{PSC} = 0.49$ in the test case with $P_{gen}^{PSC} = 30\,kW$. Secondly, the value for the upper rotational speed threshold Ω_U for the $P_{gen}^{PSC} = 10\,kW$ test case is lower than for the $P_{gen}^{PSC} = 30\,kW$.

As previously mentioned, the control algorithm was designed for unidirectional flow. Nevertheless, in bidirectional flow, the robustness of the PSC was, again, validated without further change in the control variables.

5.2.2. Generator control failure and the importance of the high-speed safety valve

The previous sections showed that the PSC algorithm maintained the electrical generator power PSC setting value, P_{gen}^{PSC}, and maximum rotational speed, Ω_{max}^{PSC}, either in variable unidirectional flow or under real bidirectional flow conditions. This algorithm was tested to the limit where a major electrical generator failure is simulated by losing the generator's counter torque setting point and, consequently, stopping control over the generator. In this situation, the HSSV is to act as a safety valve, closing immediately.

This test assumed that the emergency flag related to generator torque set-point loss was not activated. Therefore, the plant's central control unit was unaware of this situation, and the PSC algorithm controlled the turbine-generator speed in a runaway condition.

Fig. 13 presents the rotational speed, the available power, and the HSSV shutter position for two tests where the torque set-point was set to zero (the variable speed converter was shut down) in tests performed at Mutriku's wave power plant.

Despite its relatively low root-mean-square of the available power, there are, in both cases, some considerable amount of available power peaks during consecutive waves. No braking torque is applied, and the turbine-generator set attains the corresponding runaway speed. As shown in Fig. 13 the valve prevented over speed in the cases presented. Almost continuous valve actions were needed to ensure safe and permanent operation. Also, note that this test was dangerous for the integrity of the PTO. Therefore, the maximum rotational speed for this test was set to $\Omega_{max}^{PSC} = 250$ rad/s (and not $\Omega = \Omega_{max}$ as defined in Section 2).

The OPERA project testing did not include monitoring the power consumption of HSSV linear actuators. Still, the HSSV linear actuator current was limited to 2.4 A (230 V AC) for safety. The HSSV was actuated with four linear actuators instead of three for redundancy. Moreover, failure simulations revealed that the HSSV could be operated with just two actuators. Therefore, the maximum power consumption necessary for the linear actuators is estimated to be below 1 kW, a small fraction of the generator's rated capacity.

5.3. The road to industrialisation of peak shaving control

The industrialisation of OWC WEC devices will significantly benefit from applying the proposed HSSV and the algorithm if it is successful. The paper describes the path from the original concept of peak shaving control to validation under real conditions. The authors were involved in every stage of the development of the proposed control. This helps to understand where improvements are needed and what can be done next to achieve industrialisation. Some insights into the possible approach to achieve this goal are then given.

Although the strategy was developed in the laboratory before the sea testing, some results were only available after the tests, namely (1) how the HSSV position affects the turbine performance and (2) how fast the HSSV has to be actuated to achieve the desired result. All this work was carried out under tight time constraints as part of the OPERA European project. Some issues need to be addressed in the future. In the following, these issues are addressed.

The HSSV consists of a low-friction PEHD annular disc actuated by four high-performance linear actuators. This is a straightforward design. PSC can also be performed with subcomponents of the HSSV other than those described here. For redundancy, four actuators were used instead of three. Nevertheless, fault simulations have shown that the HSSV can be operated with only two actuators, and a test with only two actuators must be considered. In addition, other linear actuators should be tested to determine which are the most durable and have low consumption.

The power consumption of HSSV was not monitored during the OPERA project testing. It should be further analysed and included in optimising the control algorithm, as this must be taken from the final energy production. However, preliminary estimates have shown low power consumption for the current hardware solution.

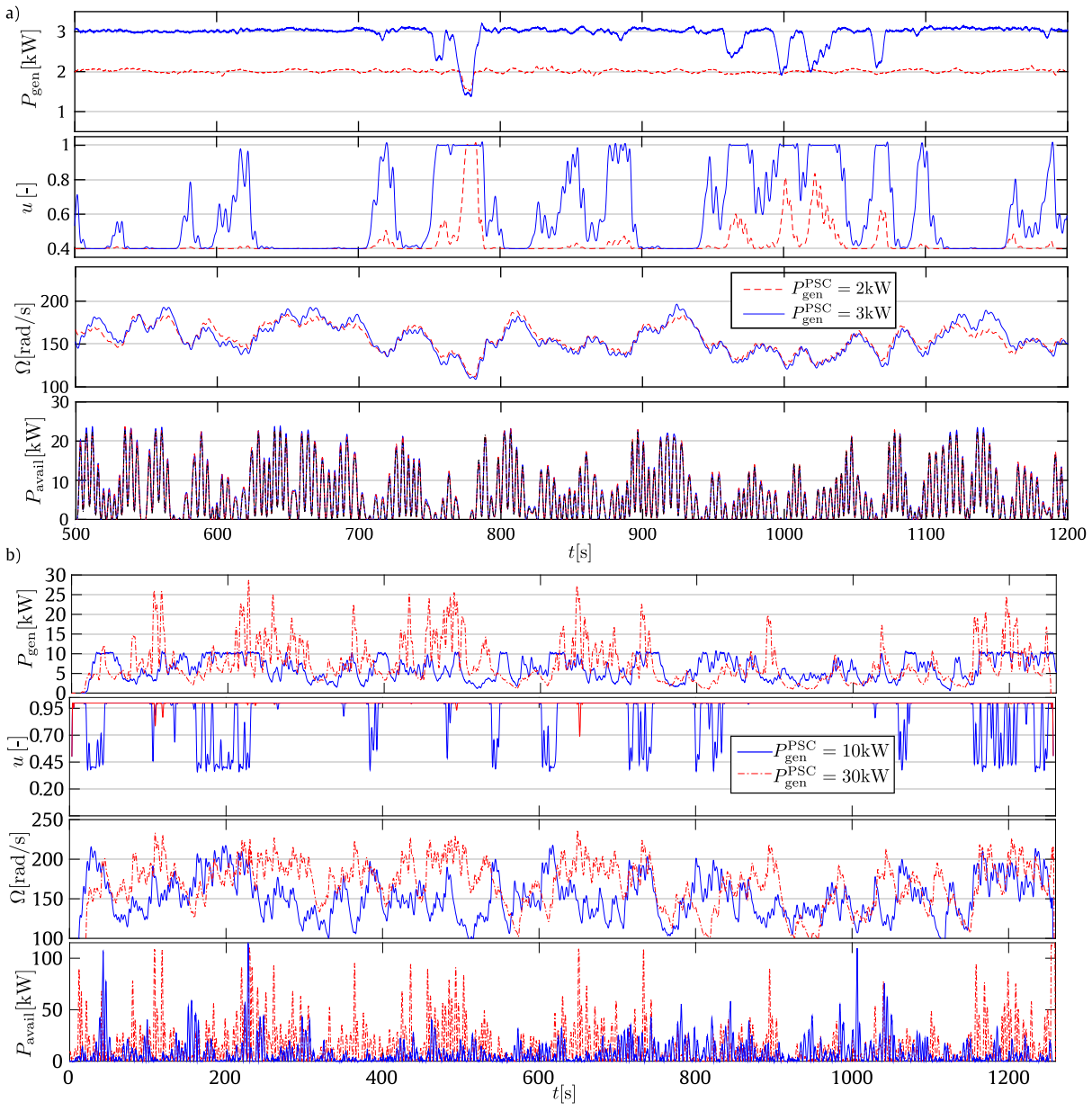

Fig. 12. Peak shaving control test results from the two test rigs: generator power, rotational speed, normalised valve position and available power as a function of time. a) IST variable flow test rig: tests using the auxiliary parametric function C and electrical generator power PSC setting values $P_{gen}^{PSC} = 2$ kW and $P_{gen}^{PSC} = 3$ kW. b) Mutriku's wave power plant: tests with $P_{gen}^{PSC} = 10$ kW and $P_{gen}^{PSC} = 30$ kW.

The PSC involves the simultaneous control of two components: the position of the HSSV shutter and the generator. A solution for both is presented here. The PSC variables need to be optimised and validated using the same control strategy. Not only to maximise the power production but also to minimise the actuation of the HSSV and reduce the actuator's wear. Further analysis must be done to evaluate the higher energy produced by actuating the HSSV compared to the OPEX/CAPEX values. Furthermore, both controls can be improved if they are optimised with the knowledge gained from this paper.

Finally, the most critical step is long-term testing under real conditions: the Mutriku wave power plant allows testing under real conditions with easy access to the PTO compared to operation and maintenance on a floating device in the open sea. This type of testing can increase investor confidence in the solution.

6. Conclusions

Two significant closely linked design variables of oscillating-water-column wave energy converters equipped with air turbines are (i) the rated power of the device and (ii) the functional operational resource window. Both are function of the predicted available power, and a fraction of the available energy is discarded when defining the most economical operational resource window. The device stops operation if the available power is too small to produce significant electrical power or is too large compared to the generator's rated power for safe operation.

A new high-speed safety valve (HSSV) was designed, constructed, and integrated into OPERA's H2020 project 30 kW biradial air turbine prototype. The valve consists of a cylindrical low-friction shutter moved by linear actuators. The valve shutter can run the whole span in less

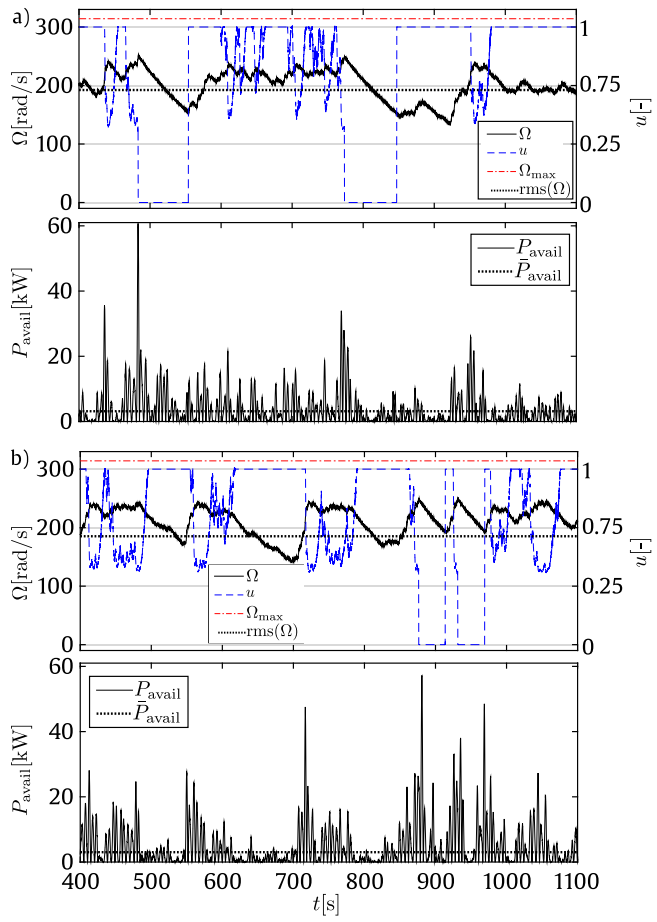

Fig. 13. Test results from Mutriku's wave power plant: time-series of the rotational speed, $\Omega(t)$ (solid black line), the normalised position of the HSSV shutter, $u(t)$ blue dashed line), and available power, $P_{\text{avail}}(t)$ (solid black line), for two test cases. The root-mean-square of the rotational speed and average available power are for test a) 191 rad/s and 3.5 kW, and for test b) 175 rad/s and 4.4 kW (dashed black lines). The red dash-dotted lines indicate the maximum allowable rotational speed.

than 0.18 s and provides possibilities for new control algorithms, like phase control or peak shaving control (PSC).

The paper describes and analyses the novel PSC algorithm for PTO operation in highly energetic sea states. PSC was first tested at the IST variable flow test rig under benign conditions and later at Mutriku's wave power plant under real sea state conditions.

Efficiency tests with different HSSV shutter positions at the IST variable-flow test rig showed how the valve aperture drastically affects the turbine performance curves. Nevertheless, the HSSV shutter position does not change the power coefficient curve as a function of the flow coefficient. This result reveals that the angular momentum of the flow leaving the rotor remains nearly the same. Therefore, the energy per unit mass exchanged between the rotor and the fluid remains almost constant. The decrease in the overall efficiency is due to flow throttling at the valve and flow incidence losses at the rotor inlet.

The PSC algorithm prevented generator overload and turbine-generator overspeed under real bidirectional flow conditions at Mutriku's wave power plant. Furthermore, PSC avoided turbine-generator overspeed under a generator's control failure.

The generator-rated power can be significantly reduced by constraining the power available to the turbine. The power plant can operate under higher energetic sea states, thereby increasing the capacity factor and the quality of the electrical energy supplied to the grid.

It should be noted that the hardware solution presented was developed as part of the OPERA project for operation at the Mutriku wave power plant and in IDOM's MARMOK-A5 floating wave energy converter in the BiMEP test site. PSC can also be performed with other HSSV subcomponents. Moreover, optimisation of the PSC control variables is required. In addition to increasing the power output, the actuation of the HSSV should be minimised to reduce wear on the actuators balancing the increased energy generated by the HSSV actuation with the OPEX and CAPEX.

CRediT authorship contribution statement

A.A.D. Carrelhas: Conceptualization, Investigation, Methodology, Software, Validation, Formal analysis, Post-processing, Visualization, Writing – original draft. **L.M.C. Gato:** Conceptualization, Investigation, Methodology, Validation, Formal analysis, Post-processing, Supervision, Resources, Funding acquisition, Writing – original draft. **J.C.C. Henriques:** Conceptualization, Investigation, Methodology, Validation, Software, Supervision, Writing – original draft.

Declaration of competing interest

The authors declare that they have no known competing financial interests or personal relationships that could have appeared to influence the work reported in this paper.

Data availability

Data will be made available on request.

Acknowledgements

This research was partially supported by European Union's Horizon 2020 Research and Innovation Programme under Grant Agreement No. 654444 (OPERA Project) and the Portuguese Foundation for Science and Technology - FCT, through IDMEC, under LAETA, project UIDB/50022/2020. We acknowledge OPERA's partners Ente Vasco de la Energia, IDOM, Tecnalia, and Kymaner for their support during sea trials.

References

[1] Puertas R, Marti L. International ranking of climate change action: An analysis using the indicators from the Climate Change Performance Index. Renew Sustain Energy Rev 2021;148:111316. http://dx.doi.org/10.1016/j.rser.2021.111316.

[2] Mujtaba A, Jena PK, Bekun FV, Sahu PK. Symmetric and asymmetric impact of economic growth, capital formation, renewable and non-renewable energy consumption on environment in OECD countries. Renew Sustain Energy Rev 2022;160:112300. http://dx.doi.org/10.1016/j.rser.2022.112300.

[3] Liu J, Yin M, Xia-Hou Q, Wang K, Zou J. Comparison of sectoral low-carbon transition pathways in China under the nationally determined contribution and 2°C targets. Renew Sustain Energy Rev 2021;149:111336. http://dx.doi.org/10.1016/j.rser.2021.111336.

[4] Wolsink M. Distributed energy systems as common goods: Socio-political acceptance of renewables in intelligent microgrids. Renew Sustain Energy Rev 2020;127:109841. http://dx.doi.org/10.1016/j.rser.2020.109841.

[5] Nolting L, Praktiknjo A. Can we phase-out all of them? Probabilistic assessments of security of electricity supply for the German case. Appl Energy 2020;263:114704. http://dx.doi.org/10.1016/j.apenergy.2020.114704.

[6] Alizadeh M, Moghaddam MP, Amjady N, Siano P, Sheikh-El-Eslami M. Flexibility in future power systems with high renewable penetration: A review. Renew Sustain Energy Rev 2016;57:1186–93. http://dx.doi.org/10.1016/j.rser.2015.12.200.

[7] Gupta A, Davis M, Kumar A. An integrated assessment framework for the decarbonization of the electricity generation sector. Appl Energy 2021;288:116634. http://dx.doi.org/10.1016/j.apenergy.2021.116634.

[8] Guerra K, Haro P, Gutiérrez R, Gómez-Barea A. Facing the high share of variable renewable energy in the power system: Flexibility and stability requirements. Appl Energy 2022;310:118561. http://dx.doi.org/10.1016/j.apenergy.2022.118561.

[9] Bhattacharya S, Pennock S, Robertson B, Hanif S, Alam MJE, Bhatnagar D, et al. Timing value of marine renewable energy resources for potential grid applications. Appl Energy 2021;299:117281. http://dx.doi.org/10.1016/j.apenergy.2021.117281.

[10] Schweizer J, Antonini A, Govoni L, Gottardi G, Archetti R, Supino E, et al. Investigating the potential and feasibility of an offshore wind farm in the Northern Adriatic Sea. Appl Energy 2016;177:449–63. http://dx.doi.org/10.1016/j.apenergy.2016.05.114.

[11] Henriques JCC, Portillo JCC, Gato LMC, Gomes RPF, Ferreira DN, Falcão AFO. Design of oscillating-water-column wave energy converters with an application to self-powered sensor buoys. Energy 2016;112:852–67. http://dx.doi.org/10.1016/j.energy.2016.06.054.

[12] Robertson B, Bekker J, Buckham B. Renewable integration for remote communities: Comparative allowable cost analyses for hydro, solar and wave energy. Appl Energy 2020;264:114677. http://dx.doi.org/10.1016/j.apenergy.2020.114677.

[13] IRENA. Fostering a blue economy: Offshore renewable energy. Abu Dhabi: International Renewable Energy Agency; 2020, URL https://www.irena.org/publications/2020/Dec/Innovation-Outlook-Ocean-Energy-Technologies.

[14] Bucher R, Bryden I. Overcoming the marine energy pre-profit phase: What classifies the game-changing "array-scale success"? Int J Mar Energy 2015. http://dx.doi.org/10.1016/j.ijome.2015.05.002.

[15] Magagna D, Uihlein A. Ocean energy development in Europe: Current status and future perspectives. Int J Mar Energy 2015;11:84–104. http://dx.doi.org/10.1016/j.ijome.2015.05.001.

[16] Portillo JCC, Collins KM, Gomes RPF, Henriques JCC, Gato LMC, Howey BD, et al. Wave energy converter physical model design and testing: The case of floating oscillating-water-columns. Appl Energy 2020;278:115638. http://dx.doi.org/10.1016/j.apenergy.2020.115638.

[17] Gomes RPF, Gato LMC, Henriques JCC, Portillo JCC, Howey BD, Collins KM, et al. Compact floating wave energy converters arrays: Mooring loads and survivability through scale physical modelling. Appl Energy 2020;280:115982. http://dx.doi.org/10.1016/j.apenergy.2020.115982.

[18] Neary VS, Ahn S, Seng BE, Allahdadi MN, Wang T, Yang Z, et al. Characterization of extreme wave conditions for wave energy converter design and project risk assessment. J Mar Sci Eng 2020;8(4). http://dx.doi.org/10.3390/jmse8040289.

[19] Gato LMC, Henriques JCC, Carrelhas AAD. Sea trial results of the biradial and Wells turbines at Mutriku wave power plant. Energy Convers Manage 2022;268:115936. http://dx.doi.org/10.1016/j.enconman.2022.115936.

[20] Tedd J, Kofoed JP. Measurements of overtopping flow time series on the Wave Dragon wave energy converter. Renew Energy 2009;34:711–7. http://dx.doi.org/10.1016/j.renene.2008.04.036.

[21] Algie C, Ryan S, Fleming A. Predicted power performance of a submerged membrane pressure-differential wave energy converter. Int J Mar Energy 2017;20:125–34. http://dx.doi.org/10.1016/j.ijome.2017.09.005.

[22] Falnes J. Ocean waves and oscillating systems: Linear interactions including wave-energy extraction. Cambridge University Press; 2002, http://dx.doi.org/10.1017/CBO9780511754630.

[23] Carrelhas AAD, Gato LMC, Falcão AFO, Henriques JCC. Control law design for the air-turbine-generator set of a fully submerged 1.5 MW mWave prototype. Part1: Numerical modelling. Renew Energy 2022;181:1402–18. http://dx.doi.org/10.1016/j.renene.2021.09.011.

[24] Falcão AFO. Wave energy utilization: A review of the technologies. Renew Sustain Energy Rev 2010;14(3):899–918. http://dx.doi.org/10.1016/j.rser.2009.11.003.

[25] Falcão AFO. Modelling and control of oscillating-body wave energy converters with hydraulic power take-off and gas accumulator. Ocean Eng 2007;34(14):2021–32. http://dx.doi.org/10.1016/j.oceaneng.2007.02.006.

[26] Portillo JCC, Reis PF, Henriques JCC, Gato LMC, Falcão AFO. Backward bent-duct buoy or frontward bent-duct buoy? Review, assessment and optimisation. Renew Sustain Energy Rev 2019;112:353–68. http://dx.doi.org/10.1016/j.rser.2019.05.026.

[27] Falcão AFO, Henriques JCC, Gato LMC. Self-rectifying air turbines for wave energy conversion: A comparative analysis. Renew Sustain Energy Rev 2018;91:1231–41. http://dx.doi.org/10.1016/j.rser.2018.04.019.

[28] Halder P, Samad A, Thévenin D. Improved design of a Wells turbine for higher operating range. Renew Energy 2017;106:122–34. http://dx.doi.org/10.1016/j.renene.2017.01.012.

[29] Gato LMC, Carrelhas AAD, Cunha AFA. Performance improvement of the axial self-rectifying impulse air-turbine for wave energy conversion by multi-row guide vanes: Design and experimental results. Energy Convers Manage 2021;243:114305. http://dx.doi.org/10.1016/j.enconman.2021.114305.

[30] Pereiras B, Castro F, El Marjani A, Rodríguez MA. An improved radial impulse turbine for OWC. Renew Energy 2011;36(5):1477–84. http://dx.doi.org/10.1016/j.renene.2010.10.013.

[31] Carrelhas AAD, Gato LMC, Henriques JCC, Falcão AFO, Varandas J. Test results of a 30 kW self-rectifying biradial air turbine-generator prototype. Renew Sustain Energy Rev 2019;109:187–98. http://dx.doi.org/10.1016/j.rser.2019.04.008.

[32] Falcão AFO, Gato LMC, Henriques JCC, Borges JE, Pereiras B, Castro F. A novel twin-rotor radial-inflow air turbine for oscillating-water-column wave energy converters. Energy 2015;93:2116–25. http://dx.doi.org/10.1016/j.energy.2015.10.046.

[33] Falcão AFO, Henriques JCC. Oscillating-water-column wave energy converters and air turbines: A review. Renew Energy 2016;85:1391–424. http://dx.doi.org/10.1016/j.renene.2015.07.086.

[34] Falcão AFO, Sarmento AJNA, Gato LMC, Brito-Melo A. The Pico OWC wave power plant: Its lifetime from conception to closure 1986–2018. Appl Ocean Res 2020;98:102104. http://dx.doi.org/10.1016/j.apor.2020.102104.

[35] Salter S, Taylor J. The design of a high-speed stop valve for oscillating water columns. In: Proc. 2nd European wave power conference. Lisbon, Portugal; 1995, p. 195–202.

[36] Henriques JCC, Gato LMC. Adaptive control of the high-speed stop-valve of the Azores plant. In: Proc. 4th European wave power conference. Aalborg, Denmark; 2000.

[37] Falcão AFO, Justino PAP. OWC wave energy devices with air flow control. Ocean Eng 1999;26(12):1275–95. http://dx.doi.org/10.1016/S0029-8018(98)00075-4.

[38] Alberdi M, Amundarain M, Garrido AJ, Garrido I, Casquero O, De la Sen M. Complementary control of oscillating water column-based wave energy conversion plants to improve the instantaneous power output. IEEE Trans Energy Convers 2011;26(4):1021–32. http://dx.doi.org/10.1109/TEC.2011.2167332.

[39] Henriques JCC, Gato LMC, Lemos JM, Gomes RPF, Falcão AFO. Peak-power control of a grid-integrated oscillating water column wave energy converter. Energy 2016;109:378–90. http://dx.doi.org/10.1016/j.energy.2016.04.098.

[40] Morais FJF, Carrelhas AAD, Gato LMC. Biplane-rotor Wells turbine: The influence of solidity, presence of guide vanes and comparison with other configurations. Energy 2023;127514. http://dx.doi.org/10.1016/j.energy.2023.127514.

[41] Henriques JCC, Gomes RPF, Gato LMC, Falcão AFO, Robles E, Ceballos S. Testing and control of a power take-off system for an oscillating-water-column wave power converter. Renew Energy 2016;85:714–24. http://dx.doi.org/10.1016/j.renene.2015.07.015.

[42] Fay FX, Robles E, Marcos M, Aldaiturriaga E, Camacho EF. Sea trial results of a predictive algorithm at the Mutriku wave power plant and controllers assessment based on a detailed plant model. Renew Energy 2020;146(11):1725–45. http://dx.doi.org/10.1016/j.renene.2019.07.129.

[43] Thiebaut F, O'Sullivan D, Kracht P, Ceballos S, López J, Boake C, et al. Testing of a floating OWC device with movable guide vane impulse turbine power take-off. In: Proc. 9th European wave and tidal energy conference, Southampton, UK. 2011.

[44] Correia da Fonseca FX, Henriques JCC, Gato LMC, Falcão AFO. Oscillating flow rig for air turbine testing. Renew Energy 2019;142:373–82. http://dx.doi.org/10.1016/j.renene.2019.04.124.

[45] Carrelhas AAD, Gato LMC, Falcão AFO, Henriques JCC. Control law design for the air-turbine-generator set of a fully submerged 1.5 MW mWave prototype. Part 2: Experimental validation. Renew Energy 2021;171:1002–13. http://dx.doi.org/10.1016/j.renene.2021.02.128.

[46] OPERA - Open sea operating experience to reduce wave energy cost, contract 654444. 2023, Accessed March 2023. http://opera-h2020.eu/.

[47] Gato LMC, Maduro AR, Carrelhas AAD, Henriques JCC, Ferreira DN. Performance improvement of the biradial self-rectifying impulse air turbine for wave energy conversion by multi-row guide vanes: Design and experimental results. Energy 2021;216:119110. http://dx.doi.org/10.1016/j.energy.2020.119110.

[48] Carrelhas AAD, Gato LMC, Henriques JCC, Falcão AFO. Experimental study of a self-rectifying biradial air turbine with fixed guide-vanes arranged into concentric annular rows. Energy 2020;198:117211. http://dx.doi.org/10.1016/j.energy.2020.117211.

[49] Henriques JCC, Gato LMC, Carrelhas AAD, Varandas J. Open-sea performance and reliability of the OWC turbine and electrical equipment. Tech. rep., OPERA - Open Sea Operating Experience to Reduce Wave Energy Costs, Deliverable D3.4; 2019, URL http://opera-h2020.eu/wp-content/uploads/2019/09/OPERA_D3.4_Open-Sea_PerformanceReliability_IST_20190724_v1.0.pdf.

[50] Faÿ F-X, Pujana A, Ruiz-Minguela P, Kelly J, Mueller M, Henriques JCC, et al. Shoreline OWC wave power plant control algorithms. Tech. rep., OPERA - Open Sea Operating Experience to Reduce Wave Energy Costs, Deliverable D4.2; 2018, http://opera-h2020.eu/wp-content/uploads/2018/08/OPERA_D4.2_Shoreline-OWC_wave_power_plant_CL_TECNALIA_2018-08-10_v1.0.pdf.

[51] Kymaner - Tecnologias Energéticas, Lda. 2023, Accessed March 2023. https://kymaner.com.

[52] Carrelhas AAD, Gato LMC. Reliable control of turbine-generator set for oscillating-water-column wave energy converters: Numerical modelling and field data comparison. Energy Convers Manage 2023;282:116811. http://dx.doi.org/10.1016/j.enconman.2023.116811.

[53] Torre-Enciso Y, Ortubia I, I. López de Aguileta L, Marqués J. Mutriku wave power plant: From the thinking out to the reality. In: Proc. 8th European wave tidal energy conference, Uppsala, Sweden. 2009, p. 319–29.

[54] Air Movement and Control Association International Inc. Laboratory methods of testing fans for aerodynamic performance rating. Tech. rep., 1999, URL https://archive.org/details/gov.law.amca.210.1999.

[55] Ferreira DN, Gato LMC, Eça L, Henriques JCC. Aerodynamic analysis of a biradial turbine with movable guide-vanes: Incidence and slip effects on efficiency. Energy 2020;200:117502. http://dx.doi.org/10.1016/j.energy.2020.117502.

[56] Henriques JCC, Portillo JCC, Sheng W, Gato LMC, Falcão AFO. Dynamics and control of air turbines in oscillating-water-column wave energy converters: Analyses and case study. Renew Sustain Energy Rev 2019;112:571–89. http://dx.doi.org/10.1016/j.rser.2019.05.010.